Chapter 4

Possible Wobbling Phenomenon in ^{125}Xe

4.1 Introduction

As discussed in the introduction, wobbling motion is a special experimental signature of the triaxial nucleus, which was first predicted by Bohr and Mottelson in 1975 [45] in an even-even nucleus. A nucleus with a stable triaxial shape exhibits different moments of inertia ($\mathscr{J}_m > \mathscr{J}_l \neq \mathscr{J}_s$) along three principal axes. Therefore, the quantal rotation of such a nucleus about the three principal axes no longer remains equivalent. The triaxial nucleus favors rotation about an axis that generates the largest moment of inertia, which corresponds to the minimum energy of the system. However, at a slightly higher energy, the same axis may execute a quantized harmonic oscillation about a space-fixed angular momentum axis. This results in distinct rotational bands corresponding to the different oscillation quanta, known as wobbling phonons labeled by the number n_ω. Frauendorf and Dönau classified the wobbling mode as longitudinal wobbling mode (LW) and transverse wobbling mode (TW) on the way the angular momentum of the odd quasiparticle couples to the triaxial core [63]. They interpreted these modes by using the Particle + Triaxial Rotor (PTR) model. The first observation of wobbling was reported in 2001 in the odd-mass ^{163}Lu [50] based on the PTR model. In odd-A nuclei, in addition to the $n_\omega = 1$ wobbling

band, there exists a signature partner band of $n_\omega = 0$ yrast band with the same signature. This signature partner (SP) band occurs both in axial and triaxial nuclei. One distinguishing feature of the wobbling band, compared to a signature partner band in a triaxial nucleus, is the presence of ΔI=1 γ-ray transitions with large $E2$ admixtures between the successive wobbling bands [48, 59, 63].

The Xe (Z = 54) nuclei lie in a transitional region between spherical Sn (Z = 50) and deformed Ce (Z = 58) nuclei. This causes an unstable coexistence of deformation-dependent excitation modes. In odd-mass Xe nuclei, the unique negative parity $h_{11/2}$ neutron orbitals form the yrast rotational bands and their signature splitting features are well described by theoretical model calculations [129–131]. In addition, the second negative-parity rotational bands based on the $h_{11/2}$ neutron orbital (called the yrare bands) have also been observed. However, in contrast to the yrast band, the parameter

$$S(I) = [E(I) - E(I-1)]/2I \tag{4.1}$$

which is used to visualize the signature splitting, is inverted in the yrare ones [132]. The magnitude of $S(I)$ depends on the projection of the total angular momentum on the symmetry axis (the K quantum number). However, nonconservation of K in triaxial nuclei leads to different K mixing in the corresponding structures, and hence, the signature splitting may appear different [133]. Thus, the quantity $S(I)$ is found to be an effective tool to quantify the degree of triaxiality in atomic nuclei [134]. Since, for the Xe isotopes, triaxial shapes have been suggested [132], Moon et al. [132] addressed the existence of signature inversion with small splitting in the yrare bands of Xe isotopes. In their work of ^{125}Xe, bands 1 and 3 (as shown in Fig. 4.1) were reported as favored and unfavored signature partners having a large signature splitting. On the other hand, bands 2 and 4 were suggested to be yrare bands with small and inverted signature splitting, as a function of I with respect to that of the yrast bands.

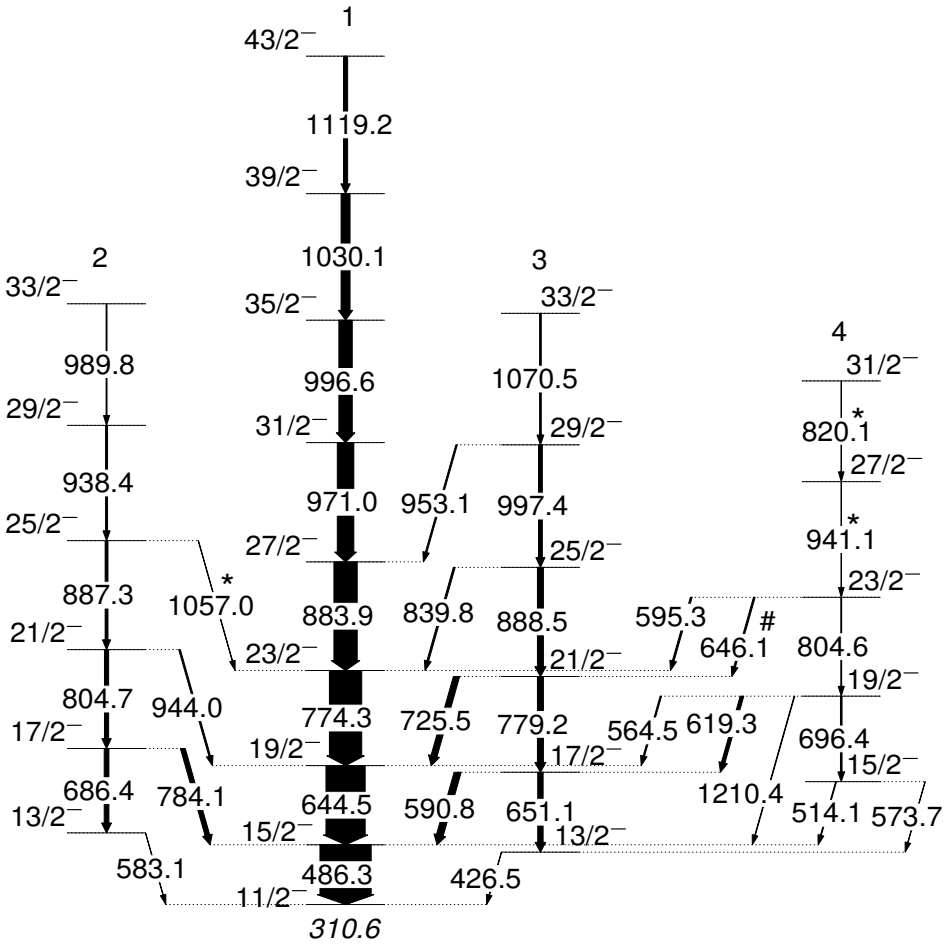

Figure 4.1 Partial level scheme of ^{125}Xe, which is mostly based on earlier works by A. Al-Khatib *et al.* and C.-B. Moon *et al.* [132, 135]. The transitions shown with "$*$" are taken from [132] as these transitions were very weak in our data. Only one new γ transition is shown with "#". To avoid contamination, the centroid of each transition was determined by gating on the nearest neighbor γ ray. The intensities of transitions in band 1 have been measured in the gate on the 486.3-keV γ ray while normalizing with respect to the intensity of the 644.5-keV one. Similarly, the intensities of transitions in bands 2, 3, and 4 were determined by gating on respective decay-out transitions. The width of each transition represents the normalized intensity of the corresponding transitions. Measurement of normalized intensity was not possible for the transitions with "$*$" and energies 426.5, 583.1, and 573.7 keV, and hence the said transitions are shown in the level scheme by arrows having a width of 1.0. For more details, see the table 4.1.

They concluded that the yrast bands originate from a $\nu h_{11/2}$ [532]7/2 configuration. Whereas, the yrare states could not be explained with a second $\nu h_{11/2}$ orbital because there is comparatively large signature splitting between $\alpha = \pm 1/2$ states across the [535]5/2 configuration. Instead, the yrare bands may be associated with the coupling of a γ phonon to the $h_{11/2}$ neutron. According to Hamamoto [136], such signature inversion can occur in a nucleus with a triaxial shape when the angular momentum of the collective rotation in the unfavored-signature states points in a direction that is different from the one specified by the large moment of inertia for a certain triaxial intrinsic shape.

However, the mass-dependent $S(I)$ values of the quasi-γ bands in even Xe isotopes are not inverted [54]. Therefore, it may not be entirely appropriate to examine the evolution of the yrare bands using such a simplistic coupling scheme.

In recent years, this type of unfavored signature partner bands based on the $\nu h_{11/2}$, $\pi h_{11/2}$, and $\pi i_{13/2}$ configurations have been revisited in ^{127}Xe [54], ^{133}La [57], ^{183}Au [47], and it was observed that these can be described by wobbling with the presence of enhanced $\Delta I = 1$, $E2$ transitions. In comparison to other mass regions, this phenomenon has been observed near A $\simeq$ 130 at a lower value of the deformation ($\varepsilon \simeq 0.16$) [54, 56, 57].

The ^{125}Xe nucleus is the nearest odd-A neighbor to ^{127}Xe, which along with ^{133}La, is known to exhibit longitudinal wobbling motion [54, 57]. All other isotopes, *i.e.*, ^{161,163,165,167}Lu [49–52], ^{135}Pr [59], ^{133}Ba [56], ^{105}Pd [60], ^{183}Au [47], exhibit transverse wobbling motion. The transverse wobbling characteristics proposed in some of the nuclei are debatable [137]. In a recent publication on ^{131}Xe by Chakraborty *etal*. [138], the authors concluded that odd-A nuclei, where a wobbling band has been observed, are mostly surrounded by two even-even nuclei with $R_E \geq 2.3$ and $Q_0 \geq 2.6$ b (where $R_E = E_{4^+}/E_{2^+}$ is the ratio of the energies of the first 2^+ and 4^+ levels and Q_0 is the intrinsic quadrupole moment. $Q_0 = 2.6$ b corresponds to $\varepsilon = 0.16$). The same is true for ^{127}Xe. The nucleus ^{125}Xe is surrounded by ^{124}Xe which has $R_E = 2.48$, $Q_0 = 3.28$ b, and ^{126}Xe

with R_E = 2.42, Q_0 = 2.8 b. It is to be noted that, as per Casten's symmetry triangle, R_E = 2.5 corresponds to γ-soft [O(6)] nuclei [102]. Thus, the magnitude of R_E and Q_0 in the neighboring even-even nuclei also makes ^{125}Xe a suitable candidate to search for wobbling motion. To confirm the wobbling motion, mixing ratios of the $\Delta I = 1$ inter-band transitions and $E2$ admixtures should be determined, as these represent an important fingerprint for wobbling.

4.2 Experimental Details

The detailed description of the experiment was published in Ref. [135] and is only briefly summarized here. Excited states of ^{125}Xe were populated in the reaction ^{82}Se(^{48}Ca, 5n)^{125}Xe at a beam energy of 205 MeV using the ATLAS accelerator at Argonne National Laboratory. Details on the target are given in Ref. [139]. The deexciting γ rays were detected with the Gammasphere array [140]. A total of 2.8×10^9 events with coincidence fold $\geq$ 5 were collected. The coincidence data were stored in γ-γ matrices, a γ-γ-γ cube, and a γ^4 hypercube. The RADWARE package [141] was used in the analysis of coincidence relationships. Two asymmetric matrices were constructed to determine the multipolarities of the γ rays, based on the directional correlation of oriented nuclei ratios (DCO ratios). The first matrix includes the events detected in forward and backward (fb) detectors at average angles of 35° and 145° on one axis, and those detected at near to $\approx$ 90° on the other, whereas the second matrix consists of events registered in detectors near to $\approx$ 90° on one axis with those detected at an average angles of 35° and 145° on the other. The DCO ratio [135] is defined as:

$$R_{DCO} = \frac{I\gamma_1 \; at \; fb, \; gated \;\; by \; \gamma_2 \; at \;\approx 90^\circ}{I\gamma_1 \; at \;\approx 90^\circ, \; gated \;\; by \; \gamma_2 \; at \; fb} \tag{4.2}$$

To measure the angular distribution of the γ rays, intensity of γ photons is measured across detectors placed along average angles of 35°, 50°, 70°, 80°, 90°, 100°, 110°, 130°,

145°, and 163° angles with respect to the beam direction. Efficiency correction was performed at each angle by using ^{182}Ta, ^{88}Y, and ^{207}Bi standard calibration sources.

Table 4.1 List of initial level energies (E_i), γ-rays energies (E_γ), spins of initial levels (I_i) and final levels (I_f), and relative intensity of the γ-transitions (I_γ) in ^{125}Xe.

E_i (keV)	E_γ (keV)	$I_i \rightarrow I_f$	I_γ
737.0 (2)	426.5	$13/2^- \rightarrow 11/2^-$	-
796.9 (2)	486.3	$15/2^- \rightarrow 11/2^-$	131.5 (71)
894.1 (7)	583.1	$13/2^- \rightarrow 11/2^-$	-
1310.7 (3)	514.1	$15/2^- \rightarrow 15/2^-$	2.15 (32)
	573.7	$15/2^- \rightarrow 13/2^-$	-
1387.9 (2)	590.8	$17/2^- \rightarrow 15/2^-$	17.4 (10)
	651.1	$17/2^- \rightarrow 13/2^-$	13.90 (78)
1441.6 (2)	644.5	$19/2^- \rightarrow 15/2^-$	100.0 (54)
1581.0 (3)	686.4	$17/2^- \rightarrow 13/2^-$	11.96 (68)
	784.1	$17/2^- \rightarrow 15/2^-$	11.45 (65)
2007.0 (3)	564.5	$19/2^- \rightarrow 19/2^-$	3.39 (40)
	619.3	$19/2^- \rightarrow 17/2^-$	8.9 (6)
	696.4	$19/2^- \rightarrow 15/2^-$	3.96 (47)
	1210.4	$19/2^- \rightarrow 15/2^-$	1.53 (20)
2167.0 (2)	725.5	$21/2^- \rightarrow 19/2^-$	15.5 (9)
	779.2	$21/2^- \rightarrow 17/2^-$	15.2 (9)
2215.9 (3)	774.3	$23/2^- \rightarrow 19/2^-$	82.6 (45)
2385.7 (3)	804.7	$21/2^- \rightarrow 17/2^-$	10.5 (6)
	944.0	$21/2^- \rightarrow 19/2^-$	4.04 (48)
2812.0 (4)	595.3	$23/2^- \rightarrow 23/2^-$	4.23 (50)
	646.1	$23/2^- \rightarrow 21/2^-$	4.11 (49)

E_i(keV)	E_γ (keV)	$I_i \rightarrow I_f$	I_γ
	804.6	$23/2^- \rightarrow 19/2^-$	2.10 (31)
3055.5 (3)	839.8	$25/2^- \rightarrow 23/2^-$	4.50 (54)
	888.5	$25/2^- \rightarrow 21/2^-$	15.2 (8)
3099.8 (3)	883.9	$27/2^- \rightarrow 23/2^-$	59.6 (32)
3273.0 (5)	887.3	$25/2^- \rightarrow 21/2^-$	7.16 (41)
	1057.0	$25/2^- \rightarrow 23/2^-$	-
3753.0 (9)	941.1	$27/2^- \rightarrow 23/2^-$	-
4052.9 (5)	953.1	$29/2^- \rightarrow 27/2^-$	3.70 (43)
	997.4	$29/2^- \rightarrow 25/2^-$	9.8 (6)
4070.8 (4)	971.0	$31/2^- \rightarrow 27/2^-$	42.3 (23)
4211.3 (8)	938.4	$29/2^- \rightarrow 25/2^-$	4.93 (59)
4573.2 (10)	820.1	$31/2^- \rightarrow 27/2^-$	-
5067.4 (5)	996.6	$35/2^- \rightarrow 31/2^-$	34.2 (25)
5123.4 (7)	1070.5	$33/2^- \rightarrow 29/2^-$	4.2 (5)
5201.1 (8)	989.8	$33/2^- \rightarrow 29/2^-$	2.19 (32)
6097.5 (4)	1030.1	$39/2^- \rightarrow 35/2^-$	22.9 (24)
7216.7 (5)	1119.2	$43/2^- \rightarrow 39/2^-$	10.4 (11)

The uncertainty in the γ-ray energy is 0.2 keV for $I_\gamma \geqslant 10$ and 0.6 keV for $I_\gamma \leq 10$.

The level energies are obtained by fitting the γ- rays energies using RADWARE software.

4.3 Results and Discussions

In the previous work, excited states in the negative-parity bands of ^{125}Xe were studied [132, 135, 142, 143]. However, no clear theoretical explanation was provided for these bands. The current study focuses on the measurement of mixing ratios of interband

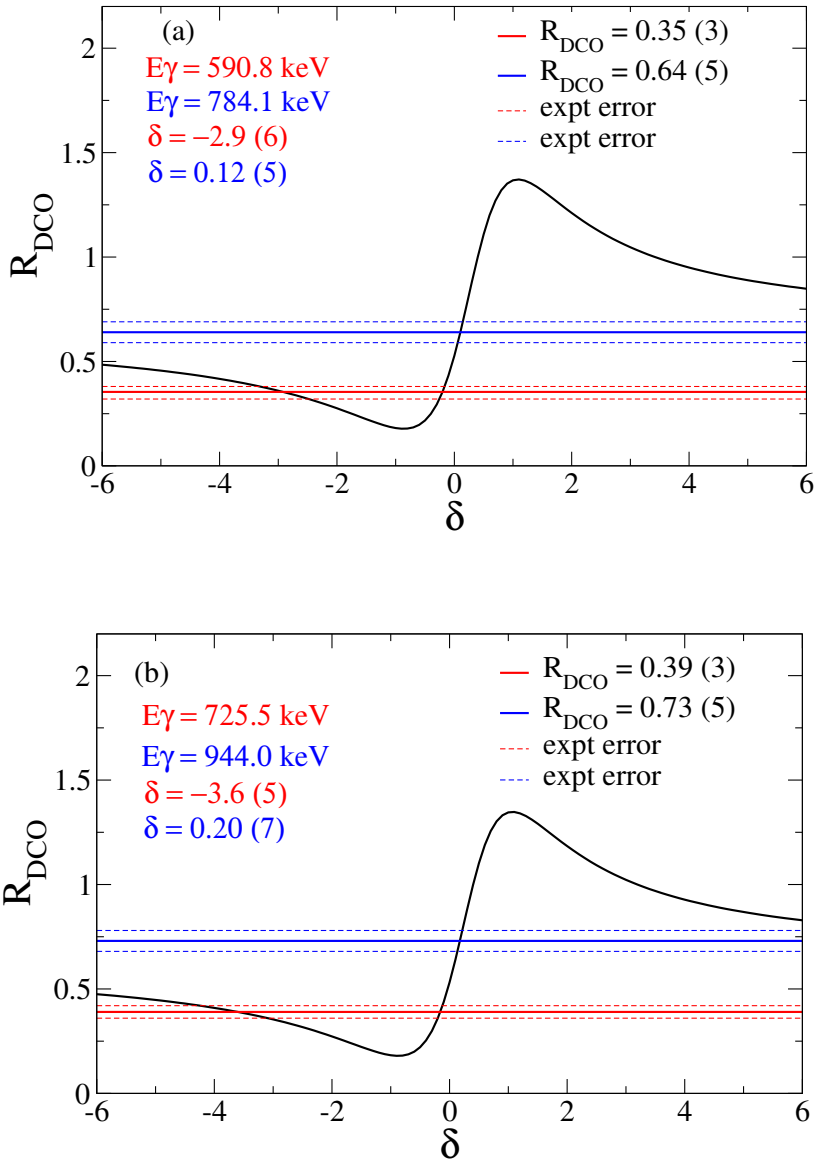

Figure 4.2 Variation of the theoretical R_{DCO} value (black line) as a function of the mixing ratio δ plotted for different $\Delta I = 1$ transitions. The red lines correspond to the experimental value of R_{DCO} for the 590.8 (panel (a))- and 725.5 (panel (b))-keV transitions decaying from band 3 to band 1. The blue lines correspond to the experimental value of R_{DCO} for the 784.1 (panel (a))- and 944.0 (panel (b))-keV transitions decaying from band 2 to band 1.

transitions at low spin, which are essential for analyzing the wobbling mode. To investigate the nature of ΔI= 1 transitions decaying from band 3 to band 1, the *DCO* ratios of these transitions were first determined. When the gating transition is of stretched quadrupole nature, the R_{DCO} value is $\approx$ 1.0 for stretched quadrupole transitions and $\approx$ 0.6 for stretched dipole ones. These ratios agree well with the assignments by Granderath *etal*. [142]. The value of the R_{DCO} depends on the detector geometry as well as on the sub-state population width(σ/j), achieved in the fusion evaporation reaction. To calculate this width, the theoretical values of R_{DCO} were calculated with the ANGCOR code [85] and were compared with the experimental values for dipole transitions at different values of (σ/j) by varying the mixing ratio (δ).

The R_{DCO} values of connecting ΔI = 1 transitions are nearly equal to those obtained by Granderath *et al.* [142], and these do not match with the typical values expected for dipole transitions, which suggests strong mixing. In Fig. 4.2(a), the theoretical R_{DCO} values are plotted as a function of δ for the 784.1- and 590.8-keV transitions ($17/2^- \rightarrow 15/2^-$, ΔI = 1). The $15/2^- \rightarrow 11/2^-$, ΔI = 2 transition with energy of 486.3 keV was employed as the gating one. The value of δ extracted for the 784.1-keV transition is 0.12 (5), and that for the 590.8-keV one is -2.9 (6). Similarly, in Fig. 4.2(b), the δ values for the 944.0- and 725.5-keV transitions are calculated. The experimental values of R_{DCO} for inter-band ΔI = 1 transitions are summarized in Table 4.2. The large values of δ for the 590.8-, 725.5-, and 839.8-keV transitions (from band 3 to band 1) indicate that they are characterized by large $E2$ admixtures.

Furthermore, the arrangement of around five to ten Compton-suppressed Ge detectors across different angles of the Gammasphere array provides an opportunity for high-statistics angular distribution measurements. The angular distribution of γ rays is given by the usual expression:

$$W(\theta) = A_0[1 + a_2 P_2(cos\theta) + a_4 P_4(cos\theta)] \tag{4.3}$$

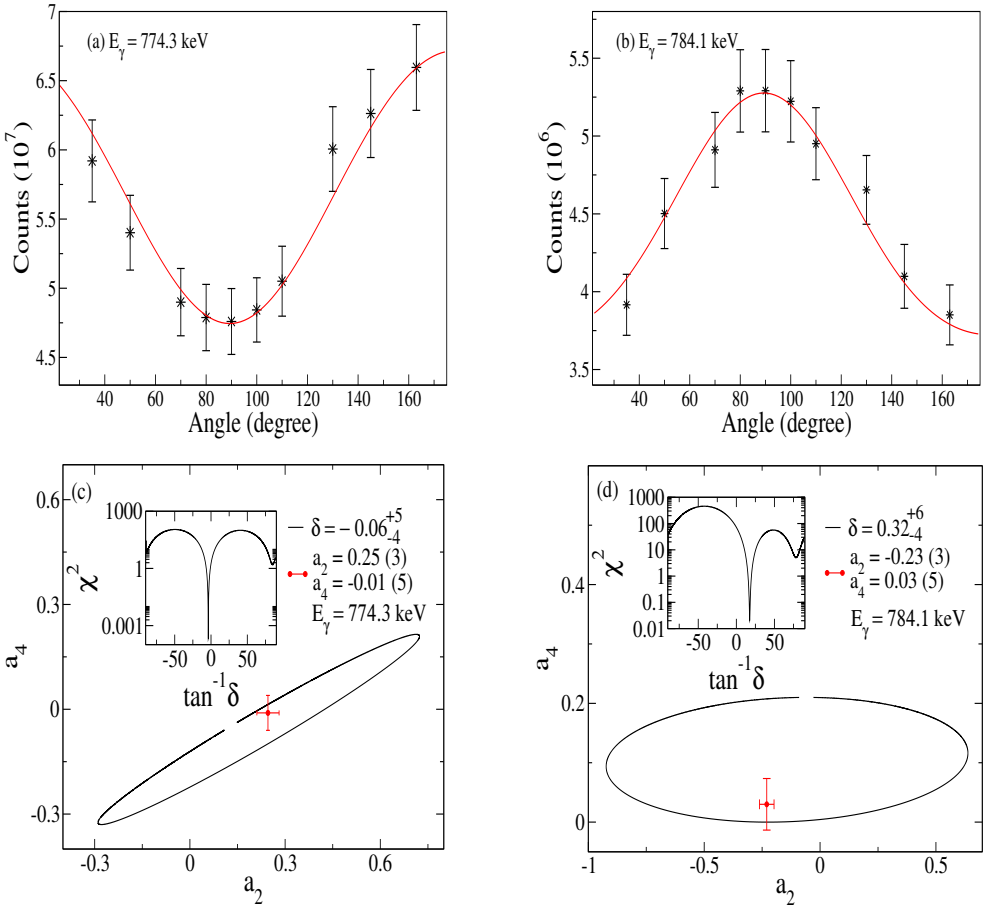

Figure 4.3 The panels (a) and (b) represent the angular distribution plots for the 774.3-keV γ ray (quadrupole transition) and the 784.1-keV γ ray (dipole transition) determined with a coincidence gate on 486.3-keV (quadrupole transition) γ ray. Panels (c) and (d) represent the a_2 - a_4 contour plots for the 774.3- and 784.1-keV transitions, respectively. The inset provides the χ^2 analysis for the experimental angular distribution of the corresponding transitions.

where a_2, a_4 are angular distribution coefficients and $P_2(cos\theta)$ and $P_4(cos\theta)$ are Legendre polynomials. The validity of the method has been established by examining the angular distribution for known stretched-$E2$ and $M1$ transitions (774.3- and 784.1-keV γ

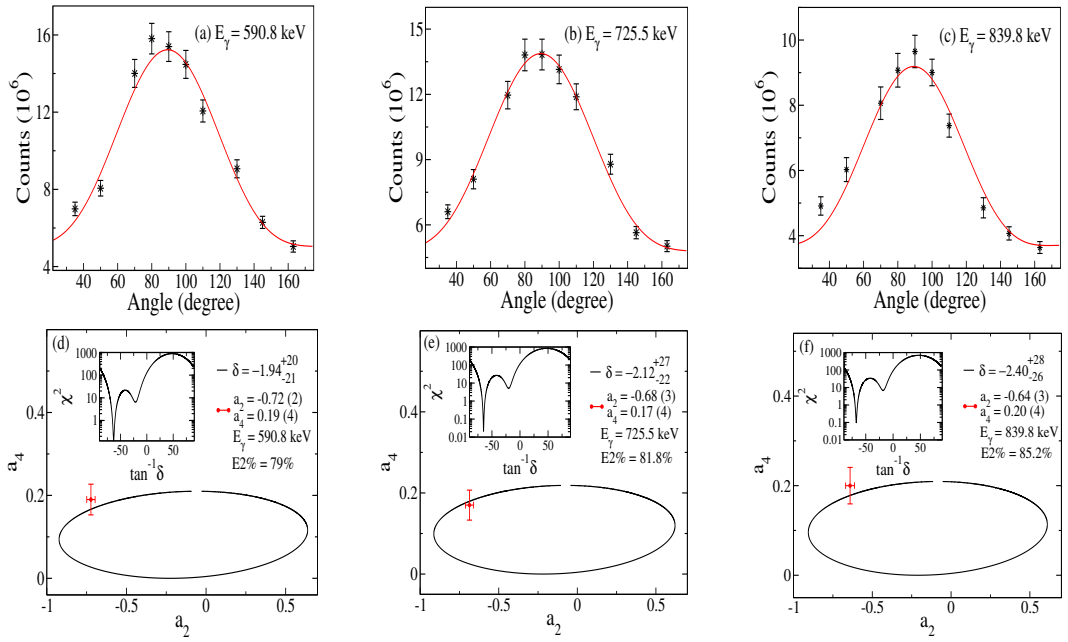

Figure 4.4 The upper panels (a), (b), and (c) represent the angular distributions for the 590.8-, 725.5-, and 839.8-keV (ΔI = 1) transitions with a coincidence gate placed on the 486.3-keV γ ray. The a_2 - a_4 contour plots of the 590.8-, 725.5-, and 839.8-keV transitions are shown in the lower panels (d), (e), and (f). The corresponding χ^2 minimization is displayed in the insets.

rays, respectively). The mixing ratios extracted for these two transitions are very small (see Fig. 4.3).

Supporting the proposed assignments, the angular distribution plots for the 590.8-, 725.5-, and 839.8-keV inter-band transitions are depicted in Figs. 4.4(a), 4.4(b), and 4.4(c), respectively. The a_2 - a_4 contour plots, along with the experimentally extracted values for these transitions, are displayed in Figs. 4.4(d), 4.4(e), and 4.4(f). It can be seen that the inter-band ΔI = 1 γ-ray transitions between bands 1 and 3 are characterized by large $E2$ admixtures, up to 85.2% (see Fig. 4.5).

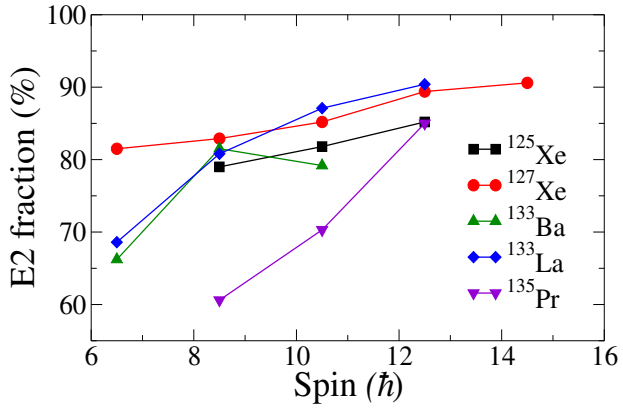

Figure 4.5 $E2$ fraction with respect to spin for $\triangle I = 1$ γ-ray transitions between $n_\omega = 1$ and $n_\omega = 0$ wobbling bands in different nuclei in the low spin regime.

Table 4.2 List of the energies of the γ transitions, spins, experimental a_2-a_4 values, R_{DCO} values, mixing ratios ($\delta_{E2/M1}$), $E2$ fractions ($= \frac{\delta^2}{1+\delta^2}$) and transition probability ratios for corresponding $\triangle I = 2$ intra- and $\triangle I = 1$ inter-band γ-ray transitions of ^{125}Xe.

$E\gamma$ (keV)	$I_i \rightarrow I_f$	a_2	a_4	R_{DCO}	$\delta^*_{E2/M1}$	$E2$ fraction(%)	$\frac{B(E2)_{out}}{B(E2)_{in}}$	$\frac{B(M1)_{out}}{B(E2)_{in}}$ ($\frac{\mu_N^2}{e^2b^2}$)
590.8	$17/2^- \rightarrow 15/2^-$	-0.72 (2)	0.19 (4)	0.35 (3)	$-1.94^{+0.20}_{-0.21}$	$79\%^{+3\%}_{-4\%}$	1.60 (17)	0.10 (2)
725.5	$21/2^- \rightarrow 19/2^-$	-0.68 (3)	0.17 (4)	0.39 (3)	$-2.12^{+0.27}_{-0.22}$	$81.8\%^{+3.3\%}_{-3.5\%}$	1.19 (12)	0.09 (2)
839.8	$25/2^- \rightarrow 23/2^-$	-0.64 (3)	0.20 (4)	0.40 (3)	$-2.40^{+0.28}_{-0.26}$	$85.2\%^{+2.5\%}_{-3.3\%}$	0.33 (5)	0.028 (5)
619.3	$19/2^- \rightarrow 17/2^-$	-0.56 (3)	0.21 (4)	0.46 (4)	$-2.81^{+0.36}_{-0.34}$	$88.7\%^{+2.3\%}_{-2.8\%}$	3.57 (54)	0.12 (3)
784.1	$17/2^- \rightarrow 15/2^-$	-0.23 (3)	0.03 (5)	0.64 (5)	$0.32^{+0.06}_{-0.04}$	$9.3\%^{+2.6\%}_{-2.1\%}$	0.045 (12)	0.190 (15)
944.0	$21/2^- \rightarrow 19/2^-$	-	-	0.73 (5)	-	-	-	-

* mixing ratio obtained from angular distribution method from the present study.

Similarly, the angular distribution plot for the 619.3-keV transition (decaying from band 4 to 3)and the corresponding a_2 - a_4 contour are shown in Figs. 4.6(a) and 4.6(b), respectively. The observed $E2$ admixture for this transition is 88.7%, which is slightly larger than that of the $\Delta I = 1$ γ-ray transitions from band 3 to band 1.

Decay transitions have been observed from band 4 to bands 3 and 1 with $\Delta I = 1$, 2, respectively. A similar pattern has been observed in ^{163}Lu [50], ^{165}Lu [51], and ^{135}Pr [59].

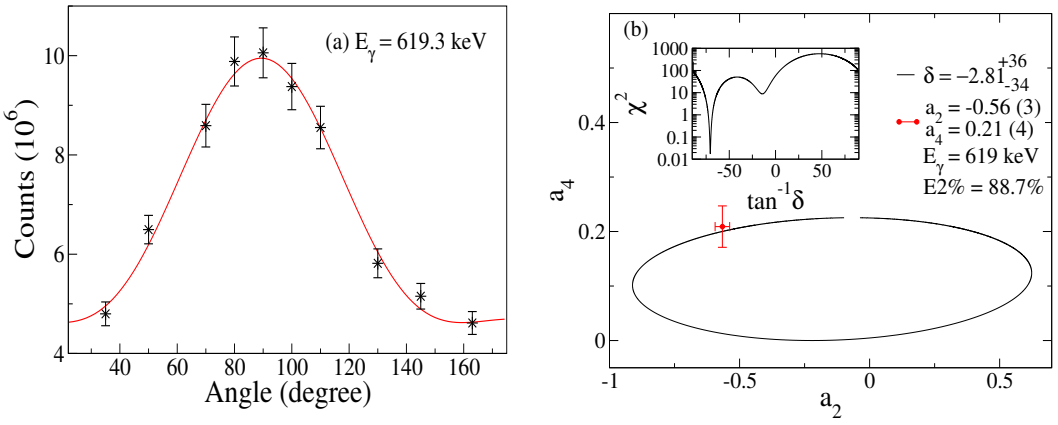

Figure 4.6 The panels (a) and (b) represent the angular distribution and a_2 - a_4 contour plot for the 619.3-keV transition with a coincidence gate on the 486.3-keV γ ray.

Furthermore, $\Delta I = 0$ transitions have also been found in ^{125}Xe which link bands 4 and 1. A similar observation was reported in ^{127}Xe [54] and ^{133}Ba [56]. A coupling between a γ-vibration and the wobbling motion was suggested to account for these observations.

To determine the $E2$ character of the linking transitions, the transition probability ratios $B(E2)_{out}/B(E2)_{in}$ were measured. These ratios, with their corresponding mixing ratios and $E2$ fractions, are summarized in Table 4.2. Small $B(M1)_{out}/B(E2)_{in}$ values were obtained, as expected for wobbling phonon bands, owing to large $E2$ transition probabilities. The large $B(E2)_{out}/B(E2)_{in}$ values also support the predominant $E2$ character of the linking transitions [47, 54, 56, 57]. The wobbling energy E$_{wobb}$ [27] is defined as

$$E_{wobb} = E(I, n_\omega = 1) - \frac{E(I-1, n_\omega = 0) + E(I+1, n_\omega = 0)}{2} \tag{4.4}$$

and is calculated here from the level energies of bands 1 and 3 in ^{125}Xe. In Fig. 6.12, E$_{wobb}$ values have been plotted for different wobbler nuclei along with ^{125}Xe. This E$_{wobb}$ value increases with spin for the ^{133}La [57], ^{127}Xe [54], and ^{125}Xe nuclei, whereas it gradually decreases for ^{133}Ba [56] and ^{135}Pr [59]. It is well known that longitudinal wobbling is characterized by wobbling energy increasing with angular momentum, whereas for transverse wobbling, E$_{wobb}$ decreases with increasing angular momentum [63]. Thus, the wobbling motion in ^{125}Xe can be categorized as longitudinal. This may be due to the

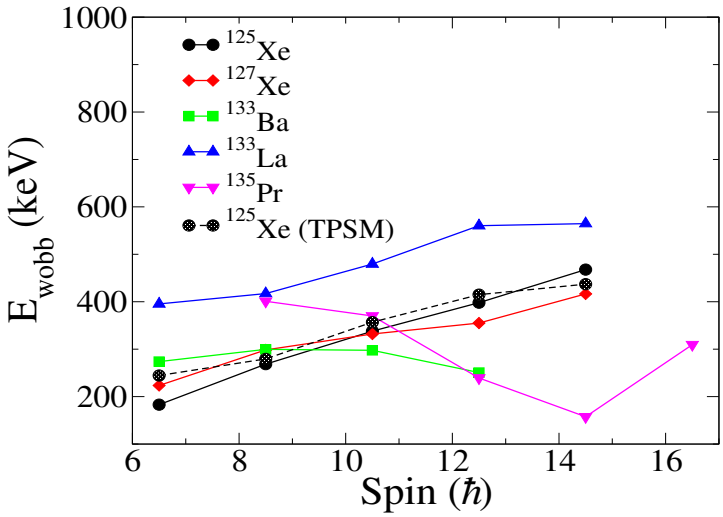

Figure 4.7 Experimentally observed E_{wobb} energies with respect to spin for ^{133}La [57], ^{127}Xe [54], ^{133}Ba [56], ^{135}Pr [59], ^{125}Xe [this work and TPSM result].

alignment of quasi-neutrons along the middle axis of the triaxial core. A similar argument was given for longitudinal wobbling in ^{127}Xe [54].

Band 2 has the same signature quantum number as band 3, but has higher excitation energies (see Fig. 4.8). This is expected for an unfavoured signature partner band of $n_\omega = 0$. One of the important characteristics of the signature partner band is the occurrence of $\Delta I = 1$, $M1$ transitions. The observed $M1$ nature of the 784.1-(see Fig. 4.3) and 944.0-keV with R_{DCO} values 0.64 (5), 0.73 (6), respectively, and 1057.0-keV transitions (refer to [132]), also supports band 2 as the unfavoured signature partner band of the $n_\omega = 0$ phonon band.

Recently, the ^{125}Xe nucleus was investigated together with the other odd-A Xe isotopes within the framework of the triaxial projected shell model (TPSM) by Jehangir *et. al.* [131]. The calculation reproduces the energy levels of the yrast and yrare bands in the various isotopes [131]. In these calculations, the basis space was expanded to include three-neutron configurations as well as configurations based on the coupling of three neutrons with two protons. This was helpful in explaining the high-spin band structures of these odd-neutron Xe isotopes. The adopted value of the axial deformation parameter (ε), along with the

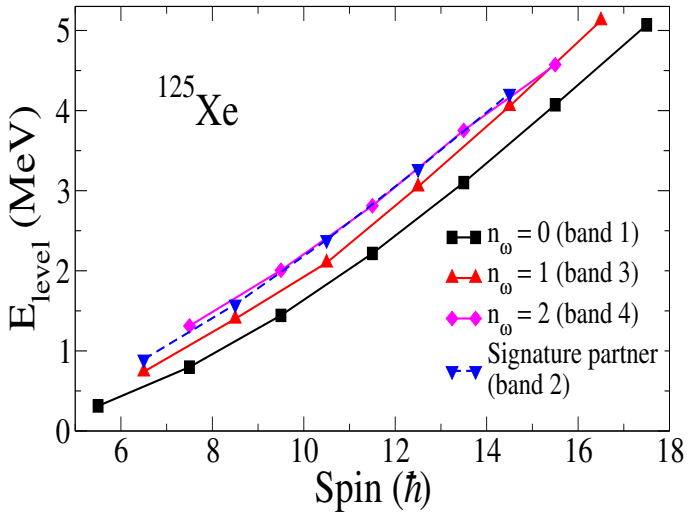

Figure 4.8 Excitation energies as a function of spin of bands 1, 2, 3, and 4 in ^{125}Xe.

γ value from the TPSM for ^{125}Xe, is given in Table I of Ref. [131]. Here, the wobbling energies were calculated by using the proposed theoretical level scheme of ^{125}Xe, based on TPSM model, and this agrees well with the experimental results (see the comparison between the observed and calculated results in Fig. 6.12). On the other hand, the mean value of the rate of change of wobbling frequency ($|\Delta\hbar\omega_{wobb}/\Delta I|$) as a function of the R_E values of the core nuclei has been plotted for the $n_\omega = 1$ wobbling band in Ref. [144]. It is observed that the value of $|\Delta\hbar\omega_{wobb}/\Delta I|$ is the largest in ^{135}Pr ($\gamma = 28^\circ$) with $R_E \sim 2.5$ [59]. However, the value of $|\Delta\hbar\omega_{wobb}/\Delta I|$ decreases monotonically with R_E deviating from the value of 2.5. The observed value of $|\Delta\hbar\omega_{wobb}/\Delta I|$ for ^{125}Xe (calculated by considering ^{124}Xe as the core nucleus) attains an intermediate value (35.84) between those of ^{135}Pr ($\gamma = 28^\circ$) and ^{133}La ($\gamma = 26^\circ$) [57]. Therefore, ^{125}Xe appears to be stabilized with a triaxial deformation of $\gamma = 27^\circ$ (according to the TPSM calculation). Thus, this nucleus shows properties of longitudinal wobbling and this observation of wobbling in ^{125}Xe further strengthens the suggested correlation between wobbling motion and R_E or Q_0, as claimed by S. Chakraborty *et al.* [138].

4.4 Summary

The directional correlation ratios and angular distributions of interconnecting transitions in the negative-parity bands (bands 1, 2, 3, and 4) of ^{125}Xe were extensively studied. Based on the findings, it is concluded that the set of four negative-parity bands originates from the coupling of a $h_{11/2}$ quasineutron with the ground state configuration of the even-even core. This coupling phenomenon drives the nucleus towards longitudinal wobbling motion and bands 1, 3, and 4 correspond to n_ω = 0, 1, and 2 wobbling phonons, respectively. Based on large $M1$ admixture and the higher excitation energy, band 2 is then identified as the unfavoured signature partner of band 1. The mixing ratios, comparatively large $E2$ fractions, and transition probability ratios are in good agreement with the expected wobbling dynamics. The observed results are found to be in agreement with the recently published calculations within the TPSM model.

***** The authors thank the ANL operations staff at Gammasphere and, in particular, J.P. Greene for help in the target preparation. M. P. would also like to thank S. Bhattacharya for his support and valuable advice. The help received from R. M. Clark, P. Fallon, T. L. Khoo, T. Lauritsen, F. Camera, P. Bringel, and C. Engelhardt in this work is gratefully acknowledged. This work is supported by the German BMBF (06 BN 109), the Alexander von Humboldt foundation, Germany, the Danish FNU Council for Natural Sciences, the US Department of Energy, Office of Science, Office of Nuclear Physics, under Contracts No. DE-AC02-06CH11357 (ANL) and No. DE-AC02-05CH11231 (LBNL), and Grants No. DE-FG02-97ER41041 (UNC), No. DE-FG02-97ER41033 (TUNL), and DE-FG02-94ER40848 (UML).